HHS Public Access

Author manuscript

J Pathol. Author manuscript; available in PMC 2021 December 11.

Published in final edited form as:

J Pathol. 2021 July ; 254(3): 289–302. doi:10.1002/path.5685.

IFT-A deficiency in juvenile mice impairs biliary development and exacerbates ADPKD liver disease

Wei Wang[1], **Tana S Pottorf**[1], **Henry H Wang**[1], **Ruochen Dong**[1], **Matthew A Kavanaugh**[1], **Joseph T Cornelius**[1], **Katie L Dennis**[2], **Udayan Apte**[3], **Michele T Pritchard**[3], **Madhulika Sharma**[4], **Pamela V Tran**[1,*]

[1]Department of Anatomy and Cell Biology, The Jared Grantham Kidney Institute, University of Kansas Medical Center, Kansas City, KS, USA

[2]Department of Pathology and Laboratory Medicine, University of Kansas Medical Center, Kansas City, KS, USA

[3]Department of Pharmacology, Toxicology and Therapeutics, The Liver Center, The Jared Grantham Kidney Institute, University of Kansas Medical Center, Kansas City, KS, USA

[4]Department of Internal Medicine, The Jared Grantham Kidney Institute, University of Kansas Medical Center, Kansas City, KS, USA

Abstract

Polycystic liver disease (PLD) is characterized by the growth of numerous biliary cysts and presents in patients with autosomal dominant polycystic kidney disease (ADPKD), causing significant morbidity. Interestingly, deletion of intraflagellar transport-B (IFT-B) complex genes in adult mouse models of ADPKD attenuates the severity of PKD and PLD. Here we examine the role of deletion of an IFT-A gene, *Thm1*, in PLD of juvenile and adult *Pkd2* conditional knockout mice. Perinatal deletion of *Thm1* resulted in disorganized and expanded biliary regions, biliary fibrosis, increased serum bile acids, and a shortened primary cilium on cytokeratin 19+ (CK19+) epithelial cells. In contrast, perinatal deletion of *Pkd2* caused PLD, with multiple CK19+ epithelial cell-lined cysts, fibrosis, lengthened primary cilia, and increased Notch and ERK signaling. Perinatal deletion of *Thm1* in *Pkd2* conditional knockout mice increased hepatomegaly, liver necrosis, as well as serum bilirubin and bile acid levels, indicating enhanced liver disease severity. In contrast to effects in the developing liver, deletion of *Thm1* alone in adult mice did not cause a biliary phenotype. Combined deletion of *Pkd2* and *Thm1* caused variable hepatic cystogenesis at 4 months of age, but differences in hepatic cystogenesis between *Pkd2*- and *Pkd2;Thm1* knockout mice were not observed by 6 months of age. Similar to juvenile PLD, Notch and ERK signaling were increased in adult *Pkd2* conditional knockout cyst-lining epithelial cells. Taken together, *Thm1* is required for biliary tract development, and proper biliary development restricts

*Correspondence to: PV Tran, Department of Anatomy and Cell Biology, The Jared Grantham Kidney Institute, University of Kansas Medical Center, 3901 Rainbow Blvd, MS #3038, Kansas City, KS 66160, USA. ptran@kumc.edu.

Author contributions statement

WW, TSP, HHW, RD, MAK, JTC, MTP and PVT performed experiments. WW, TSP, HHW, RD, MAK, JTC, KLD, UA, MTP, MS and PVT analyzed and interpreted data. WW, UA, MTP, MS and PVT designed research. WW and PVT wrote the manuscript. All authors revised the manuscript and approved the final version.

No conflicts of interest were declared.

PLD severity. Unlike IFT-B genes, *Thm1* does not markedly attenuate hepatic cystogenesis, suggesting differences in regulation of signaling and cystogenic processes in the liver by IFT-B and -A. Notably, increased Notch signaling in cyst-lining epithelial cells may indicate that aberrant activation of this pathway promotes hepatic cystogenesis, presenting as a novel potential therapeutic target.

Keywords

Ttc21b; IFT-A; biliary ciliopathy; polycystic liver disease; ADPKD; Notch signaling

Introduction

Hepatorenal fibrocystic diseases comprise a spectrum of pathologies characterized by varying degrees of cysts and fibrosis in the kidney and liver. These diseases include autosomal dominant polycystic kidney disease (ADPKD), which is among the most common, life-threatening monogenic diseases, affecting approximately 1:1000 individuals worldwide [1]. In addition to developing renal cystic disease, up to 94% of individuals with ADPKD manifest polycystic liver disease (PLD), which contributes significant morbidity [2]. In PLD, numerous fluid-filled cysts derive from the biliary ducts and progressively burden the liver, causing hepatomegaly, gastrointestinal and respiratory discomfort, and pain [3,4]. Infection and hemorrhaging of cysts can also arise. Although tolvaptan, the only FDA-approved therapy for ADPKD [5,6], attenuates the renal cystic disease, reports of its effects in the liver conflict. One case report showed reduced liver volume in an ADPKD patient [7], but several other studies indicate that tolvaptan can cause liver toxicity [6,8–10]. The paucity of therapies and conflicting reports reflect the need to continue uncovering mechanisms underlying liver fibrocystic disease.

ADPKD is caused by mutations in *PKD1* or *PKD2*, encoding polycystin proteins, which form a complex and function at the primary cilium. Mutation of *PKD1* or *PKD2* often results in deficiency of the polycystin complex in primary cilia [11,12]. These antenna-like organelles sense chemical and mechanical cues in the extracellular environment and mediate signaling pathways. In the liver, primary cilia project from the apical membrane of cholangiocytes into the biliary lumen, where they sense bile composition and flow. Primary cilia are dynamic structures built and maintained by intraflagellar transport (IFT), which mediates the bidirectional transport of protein cargo along the microtubular axoneme. IFT complex B (IFT-B) interacts with the kinesin motor to mediate anterograde IFT, whereas IFT-A together with cytoplasmic dynein is required for retrograde IFT. IFT-A also mediates ciliary entry of membrane and signaling molecules [13]. Reflecting their differential roles in ciliogenesis and maintenance, deletion of an IFT-B gene usually results in an absence of cilia [14], whereas deletion of an IFT-A gene causes shortened cilia with accumulation of proteins in a bulbous distal tip [15]. Deletion of IFT-B versus IFT-A genes can also result in differential regulation of signaling pathways.

Mutations of the IFT-B gene, *IFT56*, have been reported in families with biliary ciliopathies [16]. In mice, mutation of the IFT-B gene, *Ift88*, causes rapid expansion of

the biliary regions with an increased number of cholangiocytes and periportal fibrosis [17]. Interestingly, deletion of IFT-B genes, *Kif3a* or *Ift20*, in adult *Pkd1* conditional knockout (cko) mice, and of IFT-B gene, *Ift88* in adult *Pkd2* cko mice, attenuates both renal and biliary cystogenesis [18,19], suggesting the ciliome has therapeutic potential. The mechanisms by which cilia loss or malformation attenuates ADPKD cystogenesis remain largely undefined. Recently, P53 and Wnt signaling were reported as potential pathways suppressed by cilia mutation in *Pkd;Ift-B* mutant renal epithelial cells [19,20]. However, signaling pathways in the liver of *Pkd;Ift* double mutant mice have not been studied. Additionally, the role of IFT-A in ADPKD liver disease is unknown. To elucidate a broader mechanism of ciliopathic liver disease, we investigated the role of murine IFT-A gene, *Thm1* (*Ttc21b*), in developing and mature liver, alone and in conjunction with deletion of *Pkd2*. Homozygous mutations in *THM1* have been identified in patients with nephronophthisis [21], Meckel Syndrome [22], and renal agenesis [23], and heterozygous mutations modify the severity of Bardet–Biedl Syndrome, Jeune Syndrome, and Meckel Syndrome [21], ciliopathies that manifest fibrocystic liver disease. We have previously shown that deletion of *Thm1* results in various ciliopathy phenotypes, including developmental defects [15], renal cystic disease [24], and obesity [25]. Here we show that *Thm1* is required for postnatal biliary tract development. Furthermore, we identify increased Notch signaling in cyst-lining cholangiocytes, suggesting aberrant activation of Notch signaling as a potential contributor to hepatic cystogenesis.

Materials and methods

Mice

Animal procedures were conducted in accordance with KUMC-IACUC and AAALAC rules and regulations.

$Thm1^{aln/+}$;$ROSA26Cre^{ERT+}$ male mice were mated with $Thm1^{flox/flox}$ females to create $Thm1^{aln/flox}$;$ROSA26\text{-}Cre^{ERT+}$ (*Thm1* cko) offspring carrying one constitutive null allele and one tamoxifen-inducible floxed allele [24]. $Pkd2^{flox}$ alleles (Stock 017292, Jackson Laboratory, Bar Harbor, ME, USA) were introduced to generate $Thm1^{flox/flox}$;$Pkd2^{flox/flox}$ or $Thm1^{flox/flox}$;$Pkd2^{flox/+}$ females and $Pkd2^{flox/flox}$;$Thm1^{aln/+}$, $ROSA26\text{-}Cre^{ERT/+}$ males, which were crossed. To generate early onset models, nursing mothers were injected intraperitoneally at postnatal day 0 (P0) with tamoxifen (8 mg/40 g; T5648, Sigma-Aldrich, St. Louis, MO, USA). Progeny were sacrificed at P21. To generate late-onset models, offspring were injected intraperitoneally at P28 with tamoxifen and sacrificed at 4 or 6 months of age. Mouse genotypes and recombination of the $Thm1^{flox}$ allele were ascertained by PCR [15,24,26] (see supplementary material, Figure S1A). All mouse lines were maintained on a pure C57BL6/J background.

Bilirubin and bile acid assays

Mice were anesthetized using a ketamine-xylazine cocktail, and blood was retrieved by cardiac puncture into Microvettes (CB 300 Z, Sarstedt, Newton, NC, USA), which were centrifuged at 1000 × *g* for 10 min to obtain serum. Total bilirubin and total bile acid levels were determined using a bilirubin assay kit (MAK126, Sigma-Aldrich) and a Mouse Total

Bile Acids Assay Kit (80471, Crystal Chem, Elk Grove Village, IL, USA), with a μQuant microplate reader (BioTek Instruments, Winooski, VT, USA).

Liver and body weight measurements

Mice were weighed and livers were dissected and weighed using a standard laboratory weighing scale at the time of euthanasia. Liver weight/body weight ratios were calculated as liver weight divided by body weight for each mouse.

Histology and analyses

The left lobe of the liver was fixed in 10% formalin for several days, then processed in a tissue processor and embedded in paraffin wax. Tissue sections (7 μm) were cut using a microtome, deparaffinized, and rehydrated through an ethanol series, then stained with H&E or picrosirius red [27]. Histology was imaged using a Nikon 80i microscope equipped with a Nikon DS-Fi1 camera (Nikon Instrument, Melville, NY, USA). The ImageJ program (National Institutes of Health, Bethesda, MD, USA) was used to quantify cystic and necrotic areas in H&E-stained sections. The percentage cystic index was calculated by dividing the area of liver cysts over the area of the whole liver section, then multiplying by 100%. The percentage of necrosis was calculated by dividing the area of liver necrotic sites over the area of the whole liver section, then multiplying by 100%.

Immunofluorescence and immunohistochemistry

Deparaffinized/rehydrated tissue sections were subjected to antigen retrieval. A staining dish containing slides immersed in sodium citrate buffer (10 mM sodium citrate, 0.05% Tween 20, pH 6.0) was placed into an Oster® steamer (Sunbeam Products, Boca Raton, FL, USA) for 15 min. Slides were then rinsed 10 times in distilled water at room temperature, washed for 5 min in PBS, incubated for 5 min in 1% SDS in PBS [28], and washed three times in PBS. Immunofluorescence was performed as described previously [29] using the primary and secondary antibodies described in supplementary material, Tables S1,S2. For immunohistochemistry, tissue sections were treated with 3% hydrogen peroxide for 30 min, washed in PBS, blocked with 1% BSA for 1 h, then incubated with primary antibodies (see supplementary material, Table S1) overnight at 4 °C. Following three washes in PBS, sections were incubated with secondary antibody for 30 min (see supplementary material, Table S2). Following three washes in PBS, tissues were incubated with ABC reagent (PK-6100, Vector Laboratories, Burlingame, CA, USA), rinsed in PBS, then incubated with SigmaFAST DAB metal enhancer (D0426, Sigma-Aldrich), and counter-stained with hematoxylin.

Measurement of mean fluorescence intensity

Fluorescent staining was imaged using a Nikon 80i microscope with a Nikon DS-Fi1 camera or a Nikon Eclipse TiE attached to an A1R-SHR confocal microscope, with an A1-DU4 detector and LU4 laser launch. ImageJ was used to measure the mean fluorescence intensity (MFI). The integrated density, which is the sum of pixel intensities, of P-ERK$^+$ cyst-lining epithelium was measured. Five regions adjacent to P-ERK$^+$ cyst-lining epithelium with low fluorescence were selected to calculate the mean background fluorescence. The MFI

was calculated by dividing the integrated density of selected cyst-lining epithelial cells over the area of selected cyst-lining epithelial cells, then subtracting the mean background fluorescence.

Measurement of the length of cilia

Tissue sections immunostained to localize cytokeratin 19 (CK19) and acetylated α-tubulin were imaged using a 60× objective lens. Images of cilia were converted to greyscale. Using ImageJ, the 'Freehand Line' tool was selected to trace the length of each cilium. Pixels were converted to μm according to the scale bar.

Isolation of biliary trees

Biliary trees of P21 mice were isolated using a two-step collagenase perfusion method [30,31]. Mice were anesthetized using a ketamine-xylazine cocktail, and livers were perfused via the inferior vena cava for 10 min at 37 °C, first with calcium- and magnesium-free HBSS (Hyclone Laboratories, Logan, UT, USA), followed by HBSS containing calcium and magnesium (Hyclone Laboratories) and 0.025 mg/ml Liberase TM (Roche, Indianapolis, IN, USA). Once the liver revealed signs of digestion (8–10 min), the liver was excised and washed in ice cold HBSS to remove hepatocytes, exposing the biliary tree, which was collected for analysis.

RT-qPCR

RNA was extracted from frozen biliary tree tissue by immersion in 1 ml Trizol and homogenizing using Bullet Blender Bead Lysis tubes (Midwest Scientific, Valley Park, MO, USA) in a Bullet Blender Storm 24 (Next Advance, Troy, NY, USA) set at speed 10 for 3 min. One microgram of RNA was converted into cDNA using Quanta Biosciences qScript cDNA mix (VWR International, Radnor, PA, USA). Then, qPCR was performed in duplicate using a CFX Connect Real-Time PCR Detection System (BioRad Laboratories, Hercules, CA, USA), Quanta Biosciences Perfecta qPCR Supermix (VWR International), and the primers in supplementary material, Table S3 [25,26,32,33].

Statistics

For the comparison of more than two groups, statistical significance ($p < 0.05$) was determined using one-way ANOVA followed by Tukey's test, or using Brown–Forsythe ANOVA followed by Dunnet's T3 test when standard deviations were significantly different between groups. For the comparison of two groups, statistical significance was determined using an unpaired *t*-test. GraphPad Prism 8 (GraphPad Software, San Diego, CA, USA) was used to perform these analyses.

Results

Thm1 loss impairs biliary development and exacerbates severity of PLD in juvenile *Pkd2* cko mice

To explore the role of IFT-A deficiency in the developing liver, we deleted *Thm1* alone or together with *Pkd2* in mice at P0 and examined liver phenotypes at P21. *Thm1* cko livers

showed expanded and disorganized biliary regions (Figure 1A), without affecting liver or body weights (Figure 1B,C). In contrast, perinatal deletion of *Pkd2* caused multiple liver cysts and increased liver weight/body weight ratios (Figure 1D). Additional deletion of *Thm1* in *Pkd2* cko mice did not alter hepatic cystogenesis, but increased liver weight/body weight ratios and multifocal necrosis (Figure 1A–F). Serum bilirubin levels were not altered in *Thm1* cko and *Pkd2* cko sera, but were elevated in *Pkd2;Thm1* dko sera (Figure 1G). Serum bile acids were elevated in *Thm1* cko sera; ranged widely in *Pkd2* cko sera; and were most elevated in *Pkd2;Thm1* dko sera (Figure 1H). Taken together, these data indicate that perinatal loss of *Thm1* alone causes liver dysfunction, and on a *Pkd2* cko background, exacerbates the liver disease.

To assess the deficiency of the *Pkd2* and *Thm1* gene products in *Pkd2* and *Thm1* cko biliary tissue, transcripts were amplified using primers 3′ of the floxed exons. Transcript levels were similar between control and mutant tissues (see supplementary material, Figure S1B,C), suggesting the conditional or *aln* alleles did not strongly induce nonsense-mediated mRNA decay. *aln* is a missense mutation that results in the absence of THM1 protein [15]. Histology of $Thm1^{aln/+}$ heterozygous livers was normal (see supplementary material, Figure S1D). Thus, the mutant liver phenotypes indicate that the Rosa26-Cre^{ERT} recombinase and *aln* strategies reduced functional protein to less than 50%.

As cysts in PLD originate from bile ducts, we immunostained liver sections for CK19, a commonly used marker for biliary epithelial cells. Following injury, hepatocytes transdifferentiating into biliary epithelial cells also express CK19 [34]. In *Thm1* cko livers, there was an increased number and a disorganization of CK19+ cells (Figure 2A). However, not all cells within the *Thm1* cko expanded biliary regions were CK19+, indicating other cell types also account for the expansion. In *Pkd2* cko and *Pkd2;Thm1* dko mice, all cyst-lining cells were CK19+.

We examined proliferation, a cellular hallmark of cystogenesis, by immunostaining for proliferating cell nuclear antigen (PCNA). In mice, livers continue to mature until around 4 weeks of age. At P21, control livers revealed the presence of some PCNA+ hepatocytes and cholangiocytes, which was similar in *Thm1* cko livers (Figure 2B). In contrast, *Pkd2* cko and *Pkd2; Thm1* dko livers showed some PCNA+ hepatocytes, but many PCNA+ cyst-lining cells, consistent with the notion that proliferation drives cystogenesis.

We next examined cellular polarity by immunostaining for pericentrin, a marker of centrioles. In control livers, pericentrin localized at the apical surface of cells lining the biliary ducts (Figure 2C). In contrast, in *Thm1* cko livers, pericentrin positioning in biliary regions was not orderly. In *Pkd2* cko and *Pkd2;Thm1* dko livers, pericentrin localized at the apical surface of cells lining the biliary lumens and cysts, and was evenly spaced across cells. Thus, loss of *Thm1* alone in biliary cells may predispose to a loss in polarity.

Thm1 loss causes biliary fibrosis

Liver fibrosis is a common feature of PLD, presenting in more than half of PLD patients [35]. To assess fibrosis, we stained liver sections with picrosirius red, which labels collagen fibers [36]. In control sections, picrosirius red was present around the blood vessels (central

vein, portal vein, hepatic arteries) and biliary structures (Figure 2D). However, in *Thm1* cko livers, picrosirius red staining was greater and extended beyond the immediate biliary region-associated structures. In *Pkd2* cko livers, even more intense staining of picrosirius red was observed surrounding hepatic cysts. A similar level of intense staining was observed in *Pkd2;Thm1* dko livers. We next immunostained for alpha-smooth muscle actin (αSMA), which labels myofibroblasts, the primary cell types that secrete extracellular matrix during fibrosis. Although αSMA was mostly detected around blood vessels in control livers, αSMA was also present in the biliary regions of *Thm1* cko livers and surrounding the cysts of *Pkd2* cko and *Thm1;Pkd2* dko livers (Figure 2E). Myofibroblasts are activated by macrophages, which contribute to proinflammatory and profibrotic processes [37]. To assess the presence of macrophages, we stained liver sections for F4/80, a mouse pan-macrophage marker. Although F4/80+ cells were present in the sinusoids across all genotypes, F4/80 + cells were also present in the biliary regions of *Thm1* cko, *Pkd2* cko, and *Pkd2;Thm1* dko livers (Figure 2F). These data suggest that *Thm1* loss causes biliary inflammation and fibrosis. Although fibrosis also accompanies early onset PLD, additional loss of *Thm1* did not exacerbate PLD fibrosis at P21.

Cholangiocyte cilia are shortened in *Thm1* cko livers, but lengthened in *Pkd2* cko livers of juvenile mice

Although primary cilia are present on bipotential hepatoblasts, from which hepatocytes and biliary cells arise, cilia are absent on differentiated hepatocytes, but present on cholangiocytes protruding into the bile ducts [38]. We examined the lengths of cholangiocyte cilia by co-immunostaining liver sections to localize acetylated α-tubulin, a marker of the ciliary axoneme, together with either CK19 or with IFT81, a component of the IFT-B complex. *Thm1* cko cholangiocyte cilia were shortened (Figure 3A,C). In contrast, *Pkd2* cko cilia were lengthened, and *Pkd2* cko cilia variability was significantly different from the control (F-test; $p < 0.05$). *Pkd2;Thm1* dko cholangiocyte cilium lengths were shortened and similar to those of *Thm1* cko cilia, with some showing accumulation of IFT81 at the distal tip, consistent with a retrograde IFT defect (see supplementary material, Figure S1E) [15]. These data suggest that deletion of *Thm1* in *Pkd2* cko mice controls cilium length in cholangiocytes.

ERK and Notch signaling are increased in *Pkd2* cko and *Pkd2;Thm1* dko cyst-lining cholangiocytes

Primary cilia mediate signaling pathways. Thus, we examined signaling pathways that are involved in PLD or in biliary development. In PLD, ERK activation in cyst-lining cholangiocytes is a major driver of cell proliferation [39]. To examine the effect of *Thm1* on this pathway in cholangiocytes, we immunostained liver sections to localize P-ERK, the activated form of ERK. In control livers and similarly in *Thm1* cko livers, less than half of biliary epithelial cells (approximately 40%) were positive for P-ERK (Figure 3B,D,E). However, in *Pkd2* cko and *Pkd2;Thm1* dko livers, approximately 62 and 90%, respectively, of cyst-lining cholangiocytes were P-ERK+. Additionally, the intensity of P-ERK staining was increased in *Pkd2;Thm1* dko cyst-lining cells relative to *Pkd2* cko. Thus, loss of *Thm1* on a *Pkd2* cko background increases ERK activation in biliary epithelial cells.

The Notch pathway is essential for biliary tract development [40] and is regulated by primary cilia [41]. Therefore, we examined Notch signaling status in the mutant livers. The Notch cascade initiates with Delta or Jagged ligands that are received by Notch receptors. Of the four Notch receptors, Notch 2 is required for cholangiocyte differentiation and tubulogenesis [42,43]. Notch receptors are cleaved by presenilin-1, forming the Notch intracellular domain. The Notch intracellular domain translocates to the nucleus to activate a transcription complex containing recombination signal binding protein for immunoglobulin kappa J region (RBPj), which drives transcription of target genes, such as *Hes1*. In *Thm1* cko biliary regions, Jagged1, Notch2, and Presenilin-1 appeared to be downregulated relative to the control (Figure 3F). In contrast, in *Pkd2* cko and *Pkd2;Thm1* dko cyst-lining cholangiocytes, Jagged1, Notch2, and Presenilin-1 were increased. To ascertain that Notch signaling is altered in the biliary tissue of these mutants, we performed RT-qPCR for *Notch2*, *Presenilin-1* (*Psen1*) and *Hes1* on RNA lysates of isolated biliary trees. In *Thm1* cko biliary extracts, *Notch2*, *Presenilin-1*, and *Hes1* transcript levels were similar to those in controls (Figure 3G–I). However, in *Pkd2* and *Pkd2;Thm1* biliary extracts, *Notch2* and *Presenilin-1* were increased, and in *Pkd2;Thm1* extracts, *Hes1* was also increased. Together, these data suggest that Notch signaling is increased in biliary cystic tissue.

Thm1 deletion in a mature liver does not affect biliary morphology nor attenuate ADPKD hepatic cystogenesis at 6 months of age

As *Ift-B* deficiency in adult *Pkd1* or *Pkd2* cko mice attenuates hepatic cystogenesis [18,19], we next examined the role of IFT-A deficiency in adult, slowly progressive PLD mouse models. We deleted *Thm1* together with *Pkd2* at P28, when livers have matured [44], and examined mutant livers at 6 months of age. Global deletion of *Thm1* once the liver has matured did not affect biliary morphology nor liver weights (see supplementary material, Figure S2), but increased body weight, consistent with its role in obesity [25]. In *Pkd2* cko mice, hepatic cysts, hepatomegaly, and increased liver weight/body weight ratios were evident (Figure 4A–D). Although female ADPKD patients are associated with more severe PLD [45], liver weight/body weight ratios were similar between male and female *Pkd2* cko mice. Loss of *Thm1* together with *Pkd2* increased liver weights in female mice, but not in male mice. However, in both females and males, hepatic cystogenesis was similar between *Pkd2* cko and *Pkd2;Thm1* dko mice (Figure 4E), suggesting that *Thm1* deletion did not affect cyst formation and progression *per se*.

All cyst-lining cells of adult *Pkd2* cko and *Pkd2;Thm1* dko livers were CK19+ (Figure 5A). Many cyst-lining cells were also positive for PCNA (Figure 5B), consistent with proliferation contributing to cystogenesis. F4/80+ and αSMA+ cells were also present surrounding the biliary cysts (Figure 5C,D), indicating the presence of macrophages and myofibroblasts, respectively, and thus, of proinflammatory and profibrotic processes. In *Thm1* cko livers, immunostaining for CK19 revealed bile duct morphology similar to that in controls (see supplementary material, Figure S2A). There was also an absence of PCNA+ and F4/80+ cells in the *Thm1* cko biliary regions, similar to the control (see supplementary material, Figure S2B,C), substantiating that loss of *Thm1* in a mature liver does not cause a biliary phenotype.

Primary cilia of CK19+ cells were shortened in *Thm1* cko mice (see supplementary material, Figure S3A,B), suggesting that deletion of *Thm1* did induce a ciliary defect. In *Pkd2* cko mice, cholangiocyte primary cilia showed a wider range of cilium lengths, with some reaching over 9 μm, whereas the maximum length of cilia in control cholangiocytes was less than 6 μm (Figure 6A,B). As in the early onset model, this variability of cilium length in *Pkd2* cko livers was significantly different from the control (F-test; $p < 0.05$). Yet, collective cilium lengths of *Pkd2* cko mice were not significantly longer than those of control mice (Figure 6A,B). *Pkd2;Thm1* dko cholangiocyte cilium lengths were shortened relative to those of the control and *Pkd2* cko mice (Figure 6A,B), suggesting that loss of *Thm1* influenced the ciliary phenotype.

Finally, although *Thm1* cko bile ducts showed an absence of P-ERK and similar intensities of Notch signaling components as the control (see supplementary material, Figure S3C), cyst-lining cells of *Pkd2* cko and *Pkd2;Thm1* dko livers showed increased P-ERK (Figure 6C) and increased expression of Jagged1, Notch2, and Presenilin-1 (Figure 6D). These data suggest that similar signaling pathways drive PLD in juvenile and adult *Pkd2* cko mice.

To assess the role of *Thm1* deletion in *Pkd2* cko mice at an earlier disease stage, we examined mutant livers at 4 months of age. Unlike *Pkd2* cko mice, liver weights and liver weight/body weight ratios of *Pkd2;Thm1* dko mice were not significantly increased (see supplementary material, Figure S5A–D), suggesting milder disease. Yet, these parameters were also not significantly reduced relative to *Pkd2* cko mice. Some, but not all, *Pkd2;Thm1* dko livers showed reduced cystogenesis, resulting in a wide range of percentage hepatic cystic areas (see supplementary material, Figure S5E). These data suggest that during early disease in a late-onset ADPKD mouse model, *Thm1* deletion may have potential to slow hepatic cystogenesis, but such attenuation is not sustained for long.

Discussion

During biliary tract development, ductal plates around the portal mesenchyme duplicate, and subsequently form tubules and elongate [46]. These tubular structures form intrahepatic bile ducts, which subsequently connect to the extrahepatic hilar duct. Cells that do not integrate into a tubular structure or intrahepatic bile ducts, or do not connect with the hilar duct, involute or lose their cholangiocyte specification and convert into hepatocytes. When these developmental events fail to occur, these unintegrated cells may contribute to ductal plate malformations and result in fibrocystic liver diseases [35,47]. In *Cpk* mice, a model of autosomal recessive PKD, which exhibits PLD, and is caused by disruption of the cilia-associated protein, cystin [48], lineage tracing of ductal plate cells revealed that these cells do differentiate into hepatocytes, but show enhanced differentiation into a biliary fate [49]. Thus, several mechanisms can go awry, leading to fibrocystic liver disease, and vary with the mutant gene [50].

In juvenile *Thm1* cko mice, we observed an increased number of CK19+ cells that were disorganized, as well as biliary fibrosis. Interestingly, this phenocopies the biliary phenotype of *Notch2* knockout mice, namely increased and disorganized pan-cytokeratin-expressing cells surrounded by fibrosis [43]. Additionally, *Notch2* knockout pan-cytokeratin+ cells

express CK19 less strongly than control biliary epithelial cells. As CK19+ intensity increases with maturation of the biliary epithelial cell, this suggests that *Notch2* knockout cells are less differentiated. Three-dimensional morphological analysis of the biliary tree in *Notch1/2* knockout and in *RBPj* knockout livers show a paucity of biliary ducts, suggesting that the expanded biliary regions observed histologically result from a lack of regression of undifferentiated cells and unconnected ducts [40]. Similarly, the expanded biliary region in *Thm1* cko livers seen in this study may result from undifferentiated ductal plates that have failed to regress. By extension, the number of functional biliary ducts may be decreased in *Thm1* cko mice, and the increased serum bile acids suggest cholestatic liver disease. Yet our data do not support that Notch signaling is downregulated in *Thm1* cko biliary regions, suggesting that another signaling or cellular defect causes the biliary phenotype. As the *Thm1* cko and *Notch2* cko phenotypes are very similar, we propose that this defect may converge with a downstream defect in *Notch2* cko mice.

In the developing epidermis, Notch signaling is mediated by primary cilia. Deletion of *Kif3a* in epidermal cells during embryogenesis results in absent primary cilia and downregulation of the Notch pathway [41]. In contrast, *Pkd2* mutant primary cilia were lengthened and showed increased activation of Notch signaling. On *Pkd1* and *Pkd2* mutant renal epithelial cells, primary cilia have been shown to be lengthened [19,51,52], and a recent report suggests that increased primary cilia lengths on PKD renal epithelial cells may facilitate activation of certain signaling pathways [20]. Consistent with this, renal epithelial primary cilia were either ablated or shortened in adult *Pkd;Ift-B* dko mice, suggesting that shortening or ablating primary cilia may result in inhibition of a pro-cystogenic pathway [18,19]. Yet unlike IFT-B genes, deletion of the IFT-A gene, *Thm1*, did not strongly suppress hepatic cystogenesis in adult *Pkd2* cko mice. Additionally, although *Thm1* deletion suppressed cilium length in *Pkd2* cko mice, these shortened *Pkd2;Thm1* dko primary cilia did not counter the increased Notch signaling in cyst-lining cholangiocytes. Elucidating the mechanism of Notch misregulation in *Pkd2*-deficient cholangiocytes would be informative and could lead to the identification of additional molecular targets. Furthermore, as IFT-B and -A proteins differentially regulate certain signaling pathways, extending the analysis of Notch regulation to *Pkd;Ift-B* dko biliary epithelial cells that show attenuated cystogenesis would also further mechanistic understanding.

In ADPKD, several pathways that are upregulated in cyst-lining renal epithelial cells, including cAMP, EGFR, and ERK signaling, are also upregulated in cyst-lining cholangiocytes [39,53,54]. In ADPKD renal cystogenesis, we have shown that cyst-lining renal epithelial cells have increased Notch signaling [55]. Here we observed that Notch signaling is increased in cyst-lining cholangiocytes of both juvenile and adult ADPKD models, suggesting that Notch signaling may be an important driver of hepatic cystogenesis as well. Consistently, increased Notch signaling is a major pathway driving cholangiocarcinoma [56,57]. In the kidney, certain underlying pathogenic mechanisms of cancer and PKD overlap [58]. Similarly, in the biliary system, aberrant activation of Notch signaling promoting proliferative disease progression may be an overlapping mechanism.

The contrasting effect on hepatic cystogenesis between the deletion of *Ift-B* genes and the deletion of *Thm1* in adult ADPKD mouse models is probably due to differing roles of

IFT-B and -A in regulating signaling pathways in the liver. Our data also reveal functional differences for *Thm1* between biliary and renal epithelial cells. Perinatal loss of *Thm1* alone does not cause liver cysts, and together with the loss of *Pkd2*, does not alter hepatic cystogenesis. Yet, in the kidney, perinatal deletion of *Thm1* causes cysts [24]. Furthermore, data from our laboratory indicate that deletion of *Thm1* in juvenile *Pkd2* cko mice affects renal cystogenesis in a tubular-dependent manner, whereas deletion of *Thm1* in adult *Pkd2* cko mice attenuates renal cystogenesis. Thus, *Thm1* has a much greater influence on cystogenesis in the kidney than in the liver. Elucidating the differences between the roles of *Thm1* in biliary versus renal epithelial cells may help to identify key protein(s) that promote cyst formation or progression. In addition to cell proliferation, fluid secretion is an essential component of cyst growth [59], and perhaps *Thm1* directly or indirectly regulates a protein that is involved in fluid secretion in the kidney but not in the liver.

In summary, our study demonstrates for the first time a role for IFT-A deficiency in liver-associated ciliopathies and provides a new genetic mouse model to study biliary development. Our data also show increased Notch signaling in PLD, revealing a pathway that warrants further exploration as a novel potential therapeutic target.

Supplementary Material

Refer to Web version on PubMed Central for supplementary material.

Acknowledgements

We thank members of the Jared Grantham Kidney Institute for helpful discussions. We also thank Jing Huang of the KUMC Histology Core and acknowledge support of this core (Intellectual and Developmental Disabilities Research Center NIH U54HD090216; COBRE NIH P30GM122731). We also thank the KUMC Liver Center Cell Isolation Core, which is supported by NIH P30GM118247. This work was also supported by a K-INBRE Summer Student Award to JTC (K-INBRE P20GM103418), P20GM103549 and P30GM118247 to MTP and UA, R01DK108433 to MS, and R01DK103033 to PVT.

References

1. Lanktree MB, Haghighi A, Guiard E, et al. Prevalence estimates of polycystic kidney and liver disease by population sequencing. J Am Soc Nephrol 2018; 29: 2593–2600. [PubMed: 30135240]
2. Hogan MC, Abebe K, Torres VE, et al. Liver involvement in early autosomal-dominant polycystic kidney disease. Clin Gastroenterol Hepatol 2015; 13: 155–164 e6. [PubMed: 25111236]
3. van Aerts RMM, van de Laarschot LFM, Banales JM, et al. Clinical management of polycystic liver disease. J Hepatol 2018; 68: 827–837. [PubMed: 29175241]
4. Starzl TE, Reyes J, Tzakis A, et al. Liver transplantation for polycystic liver disease. Arch Surg 1990; 125: 575–577. [PubMed: 2331212]
5. Torres VE, Chapman AB, Devuyst O, et al. Tolvaptan in patients with autosomal dominant polycystic kidney disease. N Engl J Med 2012; 367: 2407–2418. [PubMed: 23121377]
6. Blair HA. Tolvaptan: a review in autosomal dominant polycystic kidney disease. Drugs 2019; 79: 303–313. [PubMed: 30689194]
7. Mizuno H, Hoshino J, Suwabe T, et al. Tolvaptan for the treatment of enlarged polycystic liver disease. Case Rep Nephrol Dial 2017; 7: 108–111. [PubMed: 29034246]
8. Watkins PB, Lewis JH, Kaplowitz N, et al. Clinical pattern of tolvaptan-associated liver injury in subjects with autosomal dominant polycystic kidney disease: analysis of clinical trials database. Drug Saf 2015; 38: 1103–1113. [PubMed: 26188764]

9. Muto S, Kawano H, Higashihara E, et al. The effect of tolvaptan on autosomal dominant polycystic kidney disease patients: a subgroup analysis of the Japanese patient subset from TEMPO 3:4 trial. Clin Exp Nephrol 2015; 19: 867–877. [PubMed: 25663351]
10. Blair HA, Keating GM. Tolvaptan: a review in autosomal dominant polycystic kidney disease. Drugs 2015; 75: 1797–1806. [PubMed: 26407729]
11. Freedman BS, Lam AQ, Sundsbak JL, et al. Reduced ciliary polycystin-2 in induced pluripotent stem cells from polycystic kidney disease patients with PKD1 mutations. J Am Soc Nephrol 2013; 24: 1571–1586. [PubMed: 24009235]
12. Cai Y, Fedeles SV, Dong K, et al. Altered trafficking and stability of polycystins underlie polycystic kidney disease. J Clin Invest 2014; 124: 5129–5144. [PubMed: 25365220]
13. Fu W, Wang L, Kim S, et al. Role for the IFT-A complex in selective transport to the primary cilium. Cell Rep 2016; 17: 1505–1517. [PubMed: 27806291]
14. Huangfu D, Liu A, Rakeman AS, et al. Hedgehog signalling in the mouse requires intraflagellar transport proteins. Nature 2003; 426: 83–87. [PubMed: 14603322]
15. Tran PV, Haycraft CJ, Besschetnova TY, et al. THM1 negatively modulates mouse sonic hedgehog signal transduction and affects retrograde intraflagellar transport in cilia. Nat Genet 2008; 40: 403–410. [PubMed: 18327258]
16. Shaheen R, Alsahli S, Ewida N, et al. Biallelic mutations in tetratrico-peptide repeat domain 26 (intraflagellar transport 56) cause severe biliary ciliopathy in humans. Hepatology 2020; 71: 2067–2079. [PubMed: 31595528]
17. Zimmerman KA, Song CJ, Gonzalez-Mize N, et al. Primary cilia disruption differentially affects the infiltrating and resident macrophage compartment in the liver. Am J Physiol Gastrointest Liver Physiol 2018; 314: G677–G689. [PubMed: 29543508]
18. Ma M, Tian X, Igarashi P, et al. Loss of cilia suppresses cyst growth in genetic models of autosomal dominant polycystic kidney disease. Nat Genet 2013; 45: 1004–1012. [PubMed: 23892607]
19. Shao L, El-Jouni W, Kong F, et al. Genetic reduction of cilium-length by targeting intraflagellar transport 88 protein impedes kidney and liver cysts formation in mouse models of autosomal polycystic kidney disease. 2020; 98: 1225–1241.
20. Gerakopoulos V, Ngo P, Tsiokas L. Loss of polycystins suppresses deciliation via the activation of the centrosomal integrity pathway. 2020; 3: e202000750.
21. Davis EE, Zhang Q, Liu Q, et al. TTC21B contributes both causal and modifying alleles across the ciliopathy spectrum. Nat Genet 2011; 43: 189–196. [PubMed: 21258341]
22. Shaheen R, Sebai MA, Patel N, et al. The genetic landscape of familial congenital hydrocephalus. Ann Neurol 2017; 81: 890–897. [PubMed: 28556411]
23. Shamseldin HE, Shaheen R, Ewida N, et al. The morbid genome of ciliopathies: an update. Genet Med 2020; 22: 1051–1060. [PubMed: 32055034]
24. Tran PV, Talbott GC, Turbe-Doan A, et al. Downregulating hedgehog signaling reduces renal cystogenic potential of mouse models. J Am Soc Nephrol 2014; 25: 2201–2212. [PubMed: 24700869]
25. Jacobs DT, Silva LM, Allard BA, et al. Dysfunction of intraflagellar transport-A causes hyperphagia-induced obesity and metabolic syndrome. Dis Model Mech 2016; 9: 789–798. [PubMed: 27482817]
26. Garcia-Gonzalez MA, Outeda P, Zhou Q, et al. Pkd1 and Pkd2 are required for normal placental development. PLoS One 2010; 5: e12821. [PubMed: 20862291]
27. Jiang L, Fang P, Septer S, et al. Inhibition of mast cell degranulation with cromolyn sodium exhibits organ-specific effects in polycystic kidney (PCK) rats. Int J Toxicol 2018; 37: 308–326. [PubMed: 29862868]
28. Brown D, Lydon J, McLaughlin M, et al. Antigen retrieval in cryostat tissue sections and cultured cells by treatment with sodium dodecyl sulfate (SDS). Histochem Cell Biol 1996; 105: 261–267. [PubMed: 9072183]
29. Silva LM, Wang W, Allard BA, et al. Analysis of primary cilia in renal tissue and cells. Methods Cell Biol 2019; 153: 205–229. [PubMed: 31395380]

30. Klaunig JE, Goldblatt PJ, Hinton DE, et al. Mouse liver cell culture. I. Hepatocyte isolation. In Vitro 1981; 17: 913–925. [PubMed: 6273298]
31. Ni HM, McGill MR, Chao X, et al. Removal of acetaminophen protein adducts by autophagy protects against acetaminophen-induced liver injury in mice. J Hepatol 2016; 65: 354–362. [PubMed: 27151180]
32. Puri RV, Yerrathota S, Home T, et al. Notch4 activation aggravates NF-κB-mediated inflammation in HIV-1-associated nephropathy. Dis Model Mech 2019; 12: dmm040642. [PubMed: 31727625]
33. Lee MK, Slunt HH, Martin LJ, et al. Expression of presenilin 1 and 2 (PS1 and PS2) in human and murine tissues. J Neurosci 1996; 16: 7513–7525. [PubMed: 8922407]
34. Yanger K, Zong Y, Maggs LR, et al. Robust cellular reprogramming occurs spontaneously during liver regeneration. Genes Dev 2013; 27: 719–724. [PubMed: 23520387]
35. Fabris L, Fiorotto R, Spirli C, et al. Pathobiology of inherited biliary diseases: a roadmap to understand acquired liver diseases. Nat Rev Gastroenterol Hepatol 2019; 16: 497–511. [PubMed: 31165788]
36. Junqueira LC, Bignolas G, Brentani RR. Picrosirius staining plus polarization microscopy, a specific method for collagen detection in tissue sections. Histochem J 1979; 11: 447–455. [PubMed: 91593]
37. Wynn TA, Barron L. Macrophages: master regulators of inflammation and fibrosis. Semin Liver Dis 2010; 30: 245–257. [PubMed: 20665377]
38. Huang BQ, Masyuk TV, Muff MA, et al. Isolation and characterization of cholangiocyte primary cilia. Am J Physiol Gastrointest Liver Physiol 2006; 291: G500–G509. [PubMed: 16899714]
39. Spirli C, Okolicsanyi S, Fiorotto R, et al. ERK1/2-dependent vascular endothelial growth factor signaling sustains cyst growth in polycystin-2 defective mice. Gastroenterology 2010; 138: 360–371.e7. [PubMed: 19766642]
40. Sparks EE, Huppert KA, Brown MA, et al. Notch signaling regulates formation of the three-dimensional architecture of intrahepatic bile ducts in mice. Hepatology 2010; 51: 1391–1400. [PubMed: 20069650]
41. Ezratty EJ, Stokes N, Chai S, et al. A role for the primary cilium in Notch signaling and epidermal differentiation during skin development. Cell 2011; 145: 1129–1141. [PubMed: 21703454]
42. Tchorz JS, Kinter J, Müller M, et al. Notch2 signaling promotes biliary epithelial cell fate specification and tubulogenesis during bile duct development in mice. Hepatology 2009; 50: 871–879. [PubMed: 19551907]
43. Geisler F, Nagl F, Mazur PK, et al. Liver-specific inactivation of Notch2, but not Notch1, compromises intrahepatic bile duct development in mice. Hepatology 2008; 48: 607–616. [PubMed: 18666240]
44. Alexander B, Guzail MA, Foster CS. Morphological changes during hepatocellular maturity in neonatal rats. Anat Rec 1997; 248: 104–109. [PubMed: 9143673]
45. Cornec-Le Gall E, Alam A, Perrone RD. Autosomal dominant polycystic kidney disease. Lancet 2019; 393: 919–935. [PubMed: 30819518]
46. Huppert SS, Iwafuchi-Doi M. Molecular regulation of mammalian hepatic architecture. Curr Top Dev Biol 2019; 132: 91–136. [PubMed: 30797519]
47. Wills ES, Roepman R, Drenth JP. Polycystic liver disease: ductal plate malformation and the primary cilium. Trends Mol Med 2014; 20: 261–270. [PubMed: 24506938]
48. Hou X, Mrug M, Yoder BK, et al. Cystin, a novel cilia-associated protein, is disrupted in the cpk mouse model of polycystic kidney disease. J Clin Invest 2002; 109: 533–540. [PubMed: 11854326]
49. Beaudry JB, Cordi S, Demarez C, et al. Proliferation-independent initiation of biliary cysts in polycystic liver diseases. PLoS One 2015; 10: e0132295. [PubMed: 26125584]
50. Raynaud P, Tate J, Callens C, et al. A classification of ductal plate malformations based on distinct pathogenic mechanisms of biliary dysmorphogenesis. Hepatology 2011; 53: 1959–1966. [PubMed: 21391226]
51. Hopp K, Ward CJ, Hommerding CJ, et al. Functional polycystin-1 dosage governs autosomal dominant polycystic kidney disease severity. J Clin Invest 2012; 122: 4257–4273. [PubMed: 23064367]

52. Liu X, Vien T, Duan J, et al. Polycystin-2 is an essential ion channel subunit in the primary cilium of the renal collecting duct epithelium. Elife 2018; 7: e33183. [PubMed: 29443690]

53. Masyuk TV, Masyuk AI, Torres VE, et al. Octreotide inhibits hepatic cystogenesis in a rodent model of polycystic liver disease by reducing cholangiocyte adenosine 3′,5′-cyclic monophosphate. Gastroenterology 2007; 132: 1104–1116. [PubMed: 17383431]

54. Masyuk TV, Masyuk AI, LaRusso NF. Therapeutic targets in polycystic liver disease. Curr Drug Targets 2017; 18: 950–957. [PubMed: 25915482]

55. Idowu J, Home T, Patel N, et al. Aberrant regulation of Notch3 signaling pathway in polycystic kidney disease. Sci Rep 2018; 8: 3340. [PubMed: 29463793]

56. Zender S, Nickeleit I, Wuestefeld T, et al. A critical role for notch signaling in the formation of cholangiocellular carcinomas. Cancer Cell 2013; 23: 784–795. [PubMed: 23727022]

57. Cigliano A, Wang J, Chen X, et al. Role of the Notch signaling in cholangiocarcinoma. Expert Opin Ther Targets 2017; 21: 471–483. [PubMed: 28326864]

58. Seeger-Nukpezah T, Geynisman DM, Nikonova AS, et al. The hallmarks of cancer: relevance to the pathogenesis of polycystic kidney disease. Nat Rev Nephrol 2015; 11: 515–534. [PubMed: 25870008]

59. Mangoo-Karim R, Uchic ME, Grant M, et al. Renal epithelial fluid secretion and cyst growth: the role of cyclic AMP. FASEB J 1989; 3: 2629–2632. [PubMed: 2480260]

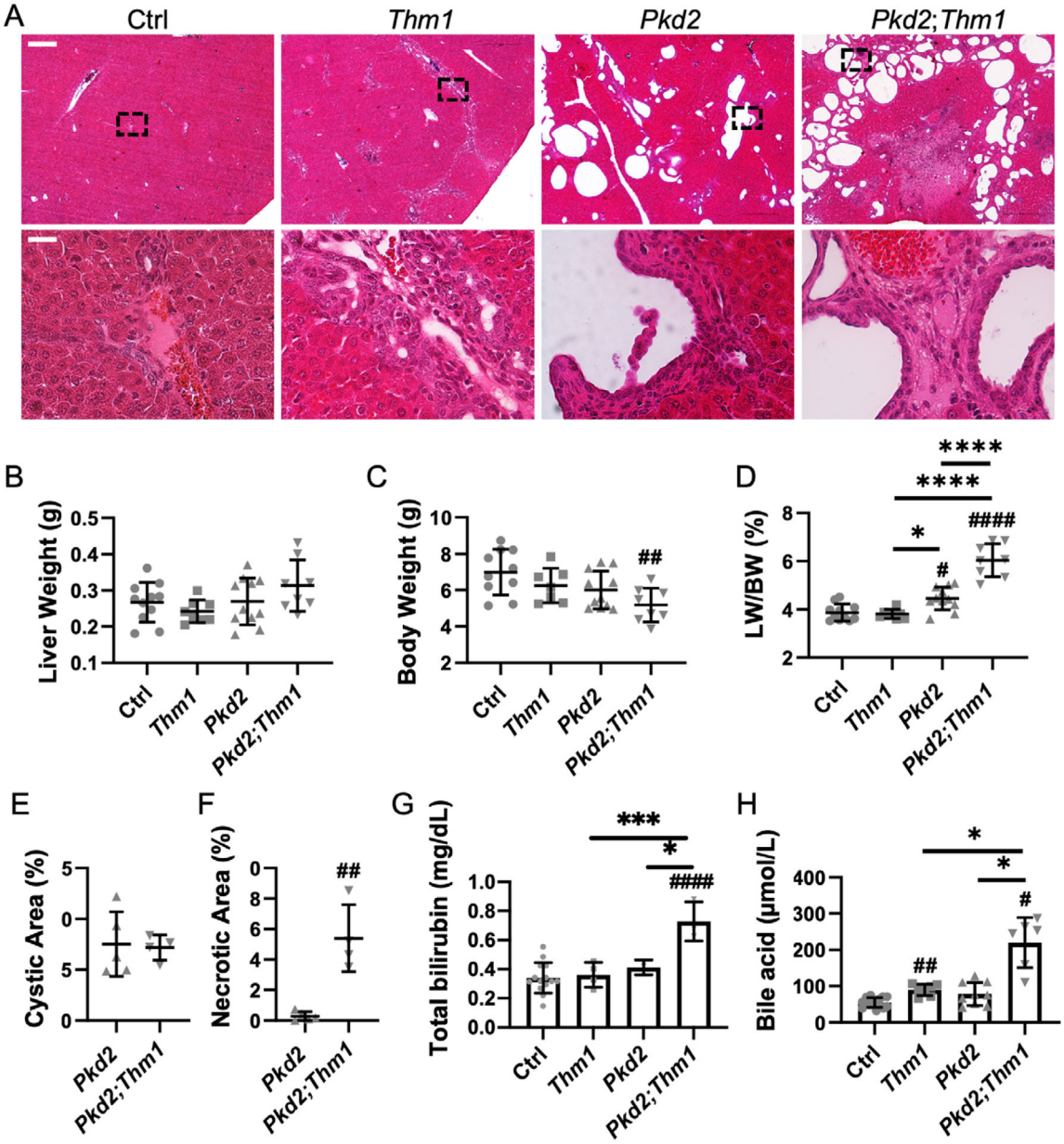

Figure 1.

Biliary defects and liver cysts of juvenile *Thm1* cko, *Pkd2* cko, and *Pkd2*;*Thm1* dko mice. (A) H&E-stained liver sections of P21 mice. Dashed boxed regions in the upper panels are shown at greater magnification in the lower panels. Scale bars: 250 μm (upper); 25 μm (lower). Arrow points to area of necrosis. $n \geq 4$ mice/genotype. (B) Liver weight; (C) body weight; (D) liver weight/body weight (LW/BW) ratios; (E) liver cystic index; (F) necrotic area (%); (G) total bilirubin; (H) bile acids. Statistical significance was determined by one-way ANOVA followed by Tukey's test in (C) and (D); unpaired *t*-test in (F); and Brown–Forsythe ANOVA followed by Dunnett's T3 test in (G) and (H). $^{\#}p < 0.05$; $^{\#\#}p < 0.01$; $^{\#\#\#\#}p < 0.0001$ relative to control or relative to *Pkd2* cko in (G). $^{*}p < 0.05$; $^{****}p < 0.0001$.

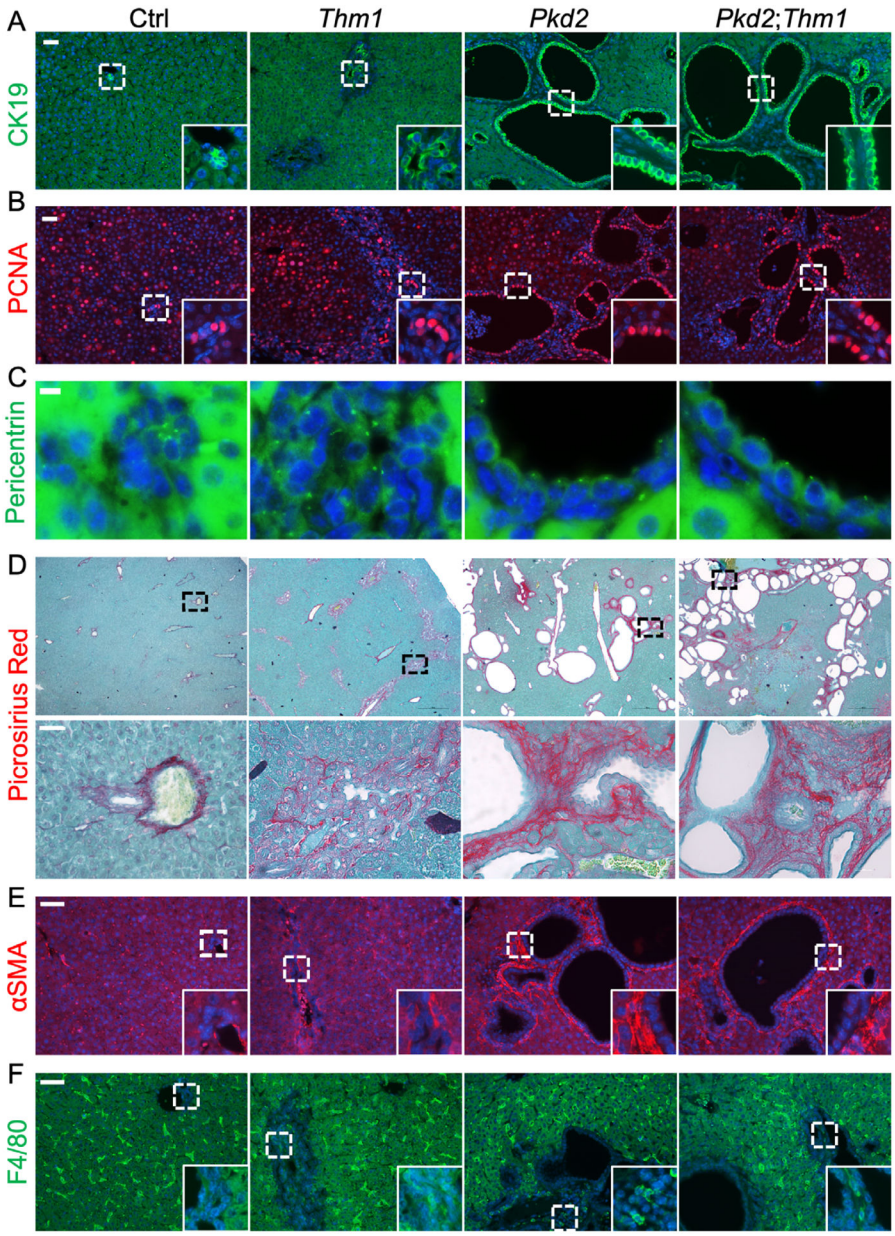

Figure 2.

Juvenile *Thm1* cko, *Pkd2* cko, and *Pkd2*;*Thm1* dko mice develop liver fibrosis. Immunofluorescence for (A) CK19+ (green); (B) PCNA (red); and (C) pericentrin (green). Nuclei are labeled with DAPI (blue). Scale bars: 50 μm in (A) and (B); 10 μm in (C). Dashed boxed regions in the main panels are shown at greater magnification in the insets. (D) Picrosirius red-stained liver sections. Dashed boxed regions in the top panels are shown at greater magnification in the bottom panels. Scale bars: 250 μm (top); 25 μm (bottom). (E) Immunofluorescence for αSMA (red) and (F) F4/80 (green). Nuclei are labeled with DAPI (blue). Scale bar: 50 μm. Dashed boxed regions in the main panels are shown at greater magnification in the insets. n = 3 mice/genotype.

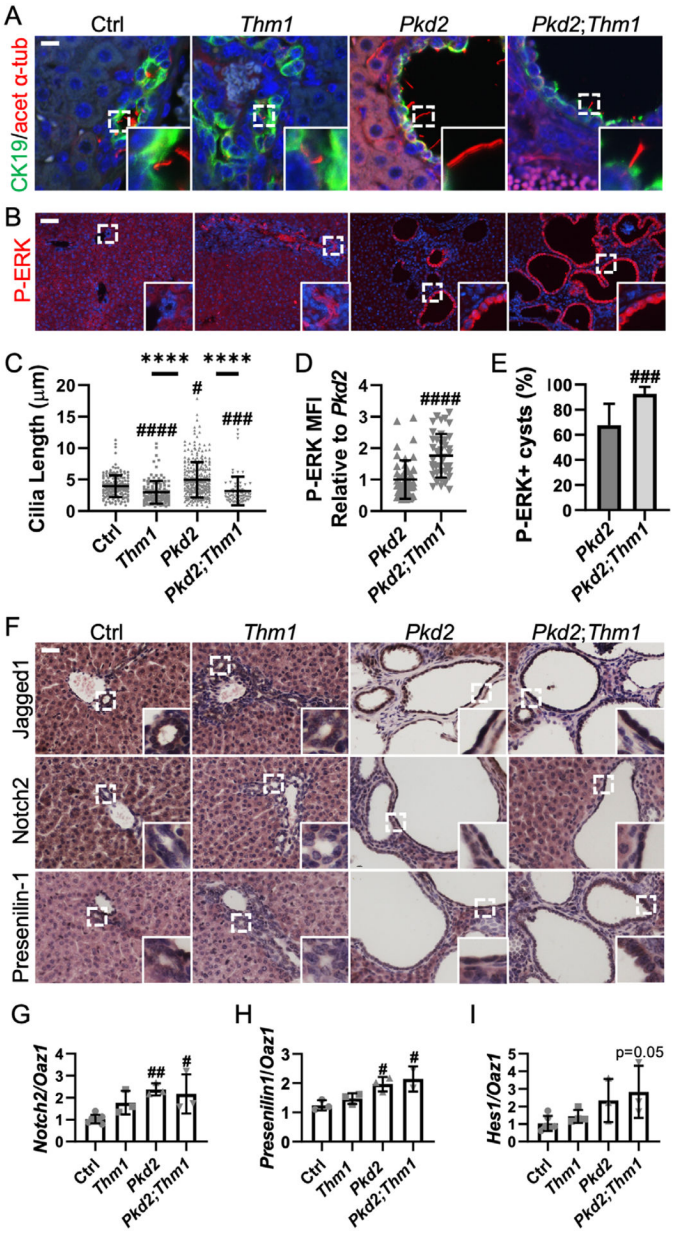

Figure 3.

Primary cilia and ERK and Notch signaling are altered in juvenile *Thm1* cko, *Pkd2* cko, and *Pkd2;Thm1* dko CK19+ cells. (A) Immunofluorescence for acetylated α-tubulin (red) and CK19 (green) of P21 mice. Nuclei are labeled with DAPI (blue). Scale bar: 10 μm. (B) Immunofluorescence for P-ERK. Nuclei are labeled with DAPI (blue). Dashed boxed regions in the main panels are shown at greater magnification in the insets. $n = 3$ mice/genotype. Scale bar: 50 μm. (C) Measurement of cholangiocyte cilium length from (A). Each data point represents an individual cilium from three mice/genotype. Bars show mean ± SD of 173 control, 133 *Thm1* cko, 312 *Pkd2* cko, and 75 *Pkd2;Thm1* dko cilia. Statistical significance was determined by ANOVA followed by Tukey's test. $^{\#}p < 0.05$; $^{\#\#\#}p < 0.001$; $^{\#\#\#\#}p < 0.0001$ relative to control; $^{****}p < 0.0001$. (D) MFI of P-ERK staining. Each

dot represents a cyst lined with P-ERK+ epithelium. Three different regions/mouse section were imaged, and 115–250 cysts were assessed for each animal. $n = 3$ mice/genotype. (E) Proportion of cysts lined with P-ERK+ epithelia. Statistical significance was determined by unpaired *t*-test. $^{###}p < 0.001$; $^{####}p < 0.0001$ relative to *Pkd2* cko. (F) Immunohistochemistry for Notch signaling components – Jagged1 ligand, Notch2 receptor, and Presenilin-1. Dashed boxed regions in the upper panels are shown at greater magnification in the insets. $n = 3$ mice/genotype. RT-qPCR for (G) *Notch2*; (H) *Presenilin-1*; and (I) *Hes1*. Statistical significance was determined by ANOVA followed by Tukey's test. $^{#}p < 0.05$; $^{##}p < 0.01$ relative to control; $p = 0.05$ relative to control; $n = 3$ mice/genotype.

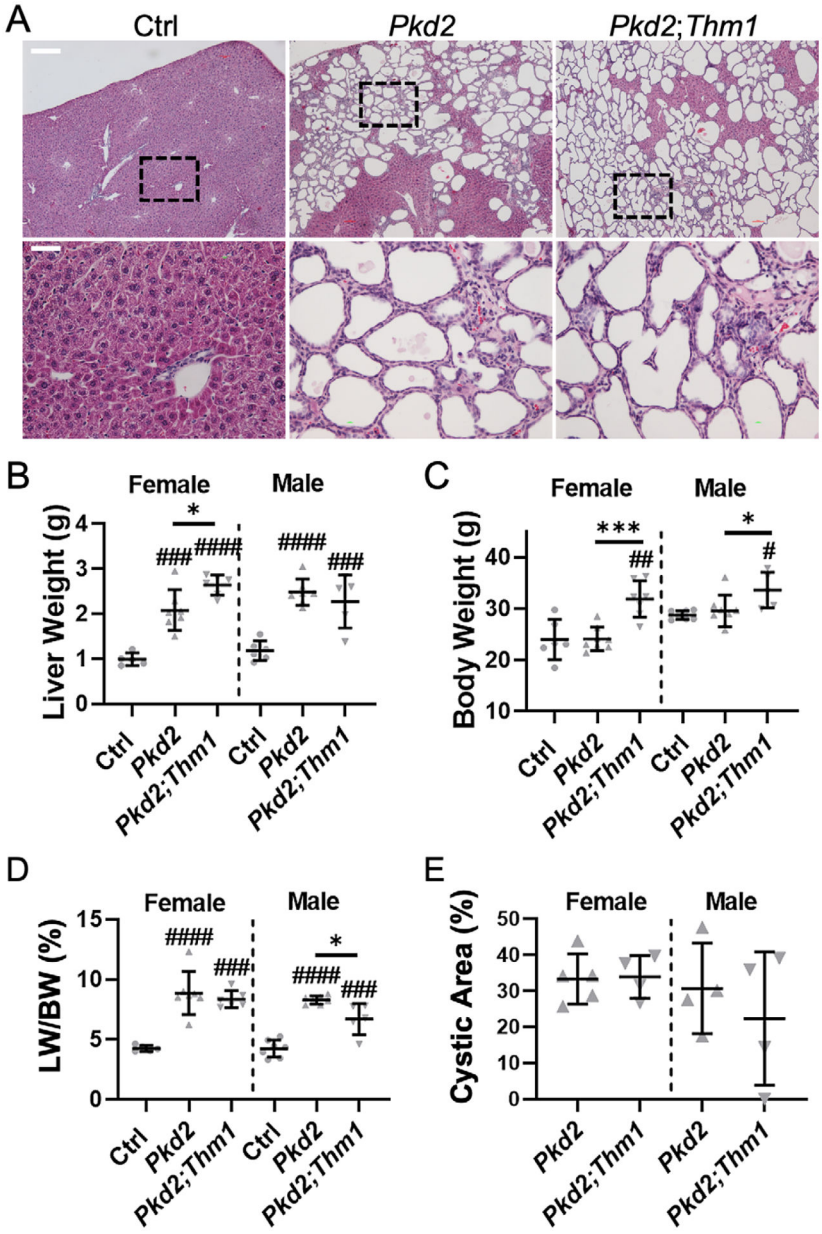

Figure 4.

Adult-onset loss of *Thm1* does not affect severity of PLD of 6-month-old *Pkd2* cko mice. (A) H&E-stained liver sections from male mice at low magnification (top panels). Dashed boxed regions are shown at greater magnification in the lower panels. Scale bars: 250 μm (top); 25 μm (bottom). (B) Liver weight; (C) body weight; (D) percentage liver weight/body weight (LW/BW); and (E) percentage cystic areas of 6-month-old female or male mice. Statistical significance was determined by ANOVA followed by Tukey's test. $^{\#}p < 0.05$; $^{\#\#}p < 0.01$; $^{\#\#\#}p < 0.001$; $^{\#\#\#\#}p < 0.0001$ relative to control; $^{*}p < 0.05$; $^{***}p < 0.001$.

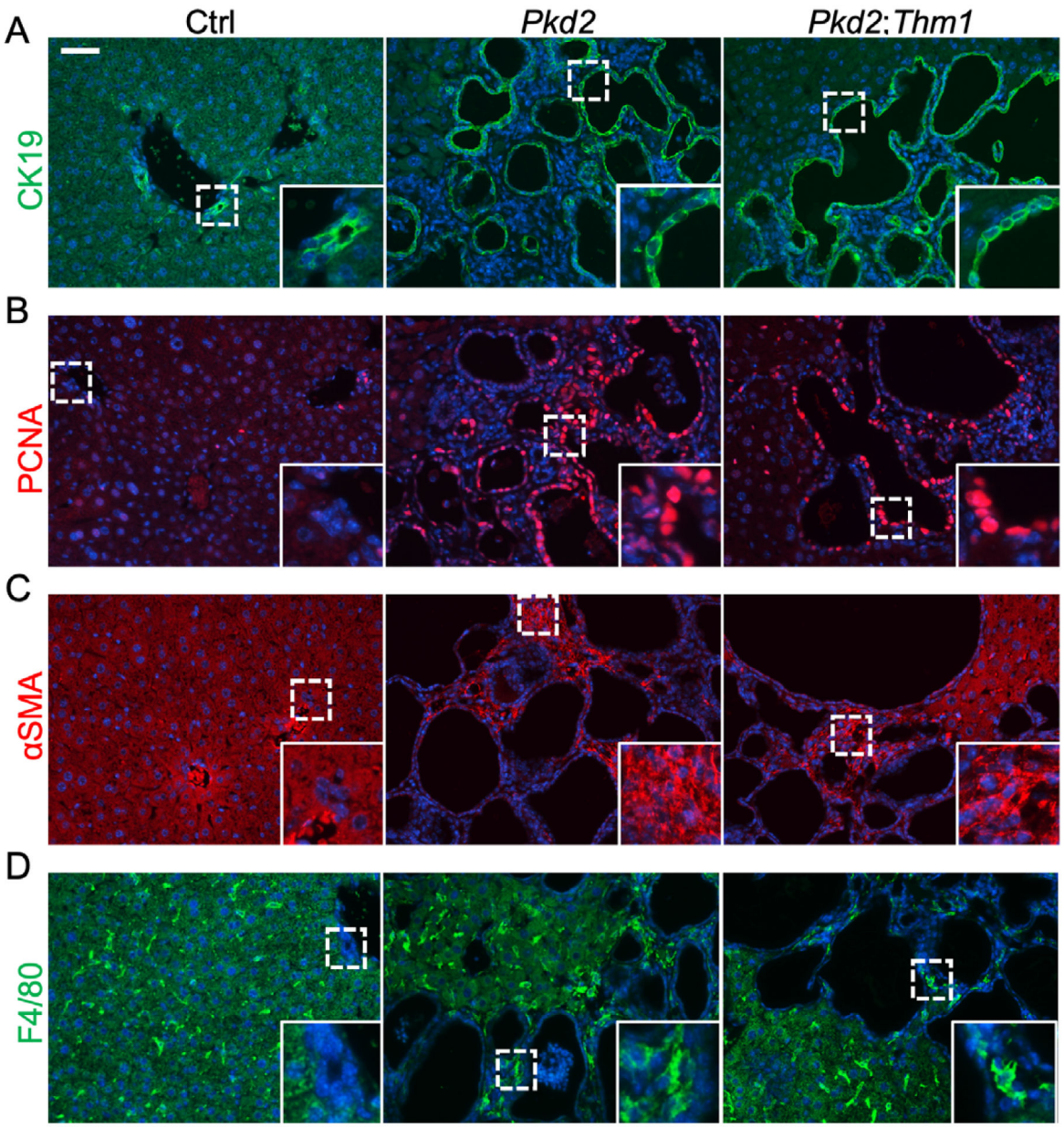

Figure 5.

Cell proliferation and inflammation are increased in PLD of adult *Pkd2* cko mice. Immunofluorescence for (A) CK19+ (green); (B) PCNA (red); (C) αSMA (red), and (D) F4/80 (green). Nuclei are labeled with DAPI (blue). Dotted boxed regions are shown at greater magnification in the insets. Scale bar: 50 μm. $n = 3$ mice/genotype.

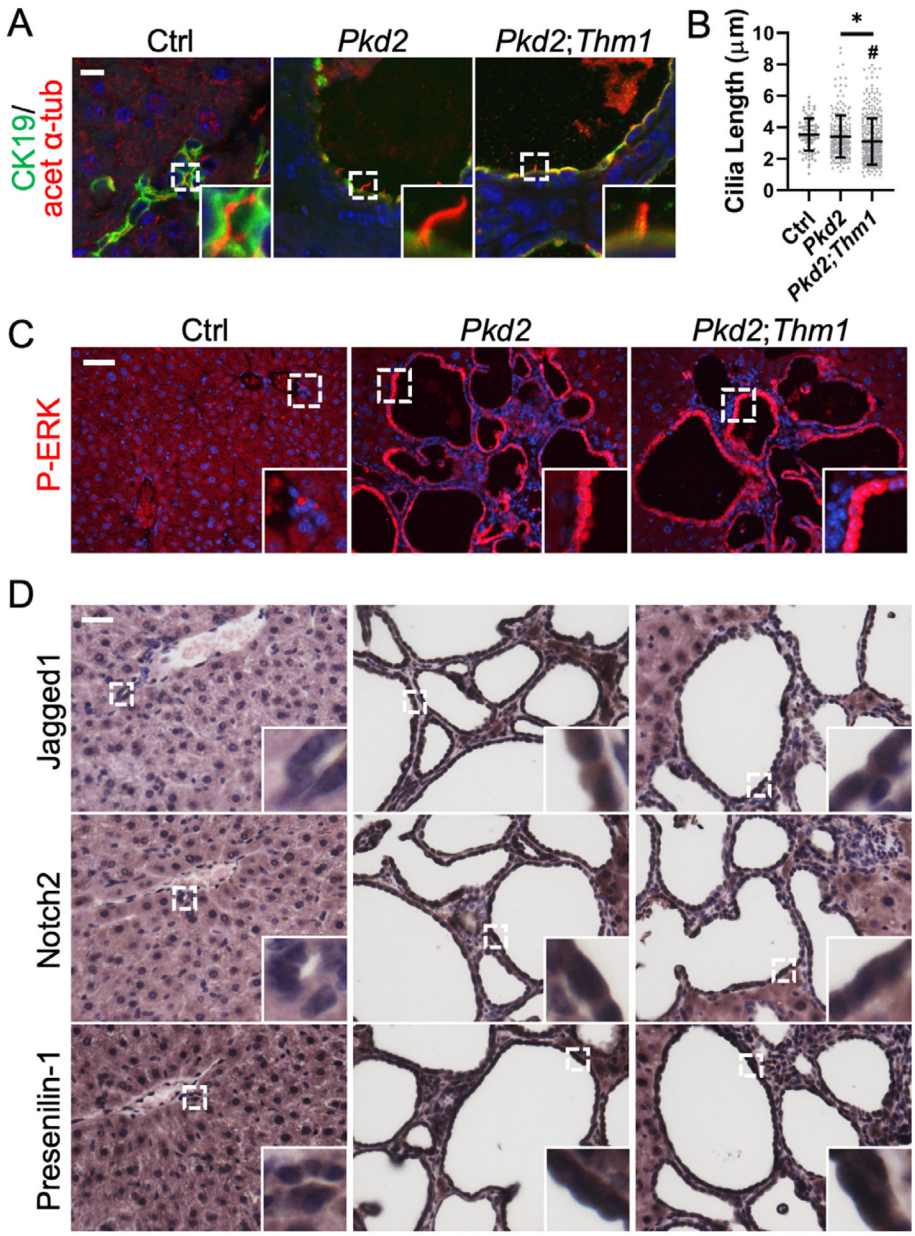

Figure 6.

ERK and Notch signaling are increased in adult *Pkd2* cko CK19+ cells. (A) Immunofluorescence for acetylated α-tubulin (red) and CK19 (green) in tissues from 6-month-old mice. Nuclei are labeled with DAPI (blue). Scale bar: 10 μm. (B) Measurement of cilium length. Each data point represents an individual cilium from four mice/genotype. Bars show mean ± SEM of 87 control, 232 *Pkd2* cko, and 361 *Pkd2;Thm1* dko cilia. Statistical significance was determined by ANOVA followed by Tukey's test. $^{\#}p < 0.05$ relative to control; $^{*}p < 0.05$. (C) Immunofluorescence for P-ERK (red). Nuclei are labeled with DAPI (blue). Dashed boxed regions in the main panels are shown at greater magnification in the insets. $n = 3$ mice/genotype. Scale bar: 50 μm. (D) Immunohistochemistry for Jagged1

ligand, Notch2 receptor, and Presenilin-1. Dashed boxed regions in the main panels are shown at greater magnification in the insets. $n = 3$ mice/genotype.